ARMA 20–1074

Issues in Determining the Crack Initiation (CI) Threshold under Confined Conditions

Sinha, S.
Colorado School of Mines, Golden, Colorado, United States
Walton, G.
Colorado School of Mines, Golden, Colorado, United States
Kim, B. H.
CDC, NIOSH, Spokane, Washington, United States

ABSTRACT: It is important to accurately identify the stress at which micro-fractures initiate in rocks under compression when studying phenomena like excavation damage zone (EDZ) formation around deep underground structures, rock burst dynamics, stability of rock slopes, etc. This stress threshold, popularly termed as the point of Crack Initiation (CI), can be determined from strain measurements or acoustic emissions monitored during laboratory compression tests. In terms of strain-based approaches, the reversal of crack volumetric strain and the point of non-linearity in the axial stress-lateral strain curve are commonly used to identify CI. There is, however, a lack of understanding as to whether these approaches are applicable/effective for CI determination under higher confinements. To shed some light on this topic, this study utilizes the two aforementioned strain-based approaches to determine CI over a wide range of confinements in context of a granitic rock, a limestone and a coal. We discuss difficulties associated with using the two approaches for cases when the lateral strain curve is non-linear from the start of the tests. Ultimately, it was found that both approaches yield similar CI estimates at low confinements, but the discrepancy between the results obtained using these approaches increases as a function of confinement. In particular, the stress at the point of axial stress-lateral strain non-linearity can be 1.5 times higher than the stress at the point of crack volumetric strain reversal.

1. INTRODUCTION

When brittle rocks are loaded in compression under a high ratio of major to minor principal stress (σ_1/σ_3; e.g. unconfined or low confinement conditions), they undergo progressive damage starting with the initiation of extensile micro-cracking, followed by microcrack interaction and coalescence that ultimate leads to the formation of a failure plane at peak strength. These distinct phases of damage are illustrated on a typical stress-strain curve in Figure 1. The stress levels at which extensile micro-cracks initiate and interact/coalesce are popularly known as Crack Initiation (CI) threshold and Crack Damage (CD) threshold, respectively. Unlike the peak strength (Hudson et al. 1972; Diederichs and Martin, 2010), CI and CD are true characteristic material parameters, meaning that they do not depend on the loading conditions employed in the test (Martin and Chandler, 1994).

CI and CD have broad design applications, especially for deep underground structures (e.g. nuclear repositories) being constructed in massive to sparsely fractured rockmasses. As a consequence of the AECL Mine-By Experiment (Martin and Read, 1996; Reed, 2004) and Aspo Pillar Experiment (Andersson and Martin, 2009; Andersson et al., 2009), CI and CD have been long treated as the lower and upper bound in-situ compressive strength, respectively (Diederichs, 2003). In particular, extensile cracking/spalling can initiate adjacent to an excavation boundary (low confinement conditions) when the tangential stresses exceed the CI threshold. Characterizing the CI under high confinements (i.e. for locations away from the excavation wall), is equally important as characterizing the CI under low confinements. This is because of the potential for connected micro-cracks to form pathways for leakage of radioactive contaminants in the Excavation Damage Zone (EDZ) (Ghazvinian, 2015; Perras and Diederichs, 2016). As one moves away from the excavation wall, the micro-cracks become less dilatant in the EDZ, but they can still affect the flow and transport properties of the rockmass (Ghazvinian, 2015). Another reason for characterizing CI is its relevance to pillar design: under low σ_3, CI plays a major role in controlling the surficial spalling process and thereby the integrity of the openings.

The CI threshold marks the onset of stable extensile microcracking in a rock specimen and can be identified by monitoring the acoustic emissions or the axial and

lateral strains during compression tests (Eberhardt et al., 1998). For the acoustic emission technique, CI corresponds to the point beyond which there is a systematic increase in crack emissions following an increase in applied stress, which is also equivalent to the point of nonlinearity in the lateral strain – axial stress curve (Eberhardt et al., 1998; Diederichs and Martin, 2010). In terms of the strain-based approaches, CI can be determined directly as the point of non-linearity in lateral strain - axial stress curve or as the point of crack volumetric strain reversal (CVSR) (Diederichs and Martin, 2010; Ghazvinian, 2010). The CVSR approach has been used extensively over the years to determine the CI for different rock types tested over a wide range of confining stresses (Andersson et al., 2009; Zhao et al., 2013; Walton et al., 2017; Peng et al., 2018; Kim et al., 2018). While most of these previous studies report CI, they do not discuss the subjectivity associated with determination of these points (it will be shown in this study that the CI determined using the CVSR and Inverse Tangent Lateral Stiffness or ITLS approaches could be different by over 150%), especially using the strain-based approaches under high confining stresses. This study is therefore an attempt to identify the issues that one might encounter while determining the CI from confined laboratory test data. For that purpose, the complete stress-strain curves for a granite (Walton, 2014), a limestone (Walton et al., 2017) and a coal (Kim et al., 2018) were examined. For the sake of completeness, the data obtained from the unconfined compressive test were also included in the analysis.

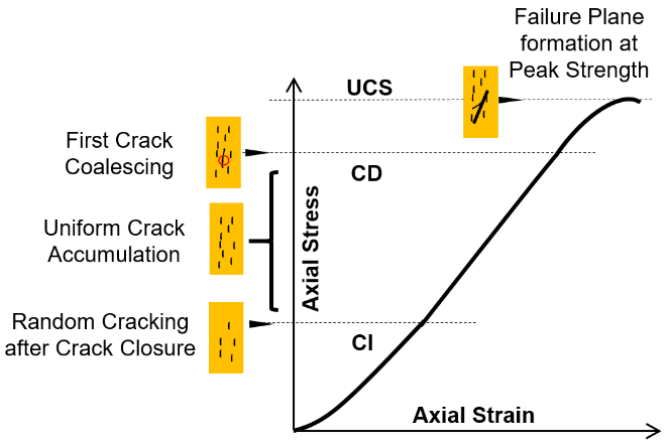

Fig. 1. Different phases of damage on a typical stress-strain curve.

2. STRAIN-BASED METHODOLOGIES FOR DETERMINATION OF CI

In this study, we consider the CVSR and ITLS (which is used to identify the point of lateral strain non-linearity; Ghazvinian, 2010) approaches only. In principle, both these approaches should yield the same CI, as the inelastic volume change is related to the lateral dilation of micro-cracks (at this point, there is no inelastic axial strain).

The CVSR approach predicts the CI to be at the point of reversal of crack volumetric strain. The crack volumetric strain ($\epsilon_{v,crack}$) can be determined by subtracting the elastic volumetric strain from the total volumetric strain (ϵ_v), accordingly to the equations given by Martin and Chandler (1994):

$$\epsilon_v = \epsilon_{axial} + 2\epsilon_{lateral} \quad (1)$$

$$\epsilon_{v,crack} = \epsilon_v - (\sigma_1 - \sigma_3)\frac{(1-2\nu)}{E} \quad (2)$$

where, ϵ_{axial} and $\epsilon_{lateral}$ are the axial and lateral strains, σ_1 and σ_3 are the major and minor principal stress, E is the Young's modulus and ν is the Poisson's ratio. As the crack volumetric strain is dependent on the elastic constants (see Eq. 2), it is important to first obtain reliable estimates of E and ν before employing the CVSR approach to determine CI (Eberhardt et al., 1998; Ghazvinian, 2010). The crack volumetric strain is sensitive particularly to the Poisson's ratio (Eberhardt et al., 1998; Ghazvinian, 2010), and it is often very difficult to determine ν from confined rock test data. The issue lies in the mismatch in the stress ranges corresponding to the linear segments of the axial and lateral strain data. In other words, the linear segment of axial strain – axial stress curve might exceed the CI while the linear segment of lateral strain - axial stress curve might include some degree of crack closure in the axial strain space. The occurrence of the former situation results in overestimation of ν, while the latter one leads to underestimation. Note that the ISRM suggested methods do not discuss this difficulty nor does it provide any solution to this problem (Bieniawski and Bernede, 1979; Fairhurst and Hudson, 1999). Recently, in one case the authors found the Poisson's ratio to be 260% higher when using the second approach in comparison to the first one (Sinha and Walton, 2020). Given the subjectivity in ν determination, the authors computed the crack volumetric strain (CVS) for a granite (tested under 60 MPa confinement) with ν of 0.1, 0.2 and 0.3 and the corresponding graphs are shown in Figure 2. As can be seen, the point of CVSR shifts significantly to the right with increase in Poisson's ratio. The amount of shift is not linearly related to ν and is controlled by the shape of the stress-strain curve.

To avoid these issues with the CVSR approach, Ghazvinian (2010) proposed the ITLS approach. The advantage of the ITLS approach is that it relies solely on the shape of the axial stress – lateral strain curve for identifying CI. The inverse tangent lateral stiffness can be calculated using the following equation (Ghazvinian, 2010):

$$\epsilon_l \Delta = \frac{\Delta\epsilon_{lateral}}{\Delta\sigma_1} \quad (3)$$

where, $\Delta\sigma_1 = \sigma_{i+8} - \sigma_{i-8}$ $(i = 1, 2, 3 \ldots)$ and σ_i is the i[th] axial stress datapoint, $\Delta\epsilon_{lateral} = \epsilon_{lateral,i+8} - \varepsilon_{lateral,i-8}$ $(i = 1, 2, 3 \ldots)$ and $\varepsilon_{lateral,i}$ is the i[th] lateral strain datapoint.

The recommended bin size of 16 can be modified depending on the resolution of test data. In this study, a bin size of 16 was employed following a moving average analysis to reduce the noise in the ITLS values. The point where the ITLS starts to deviate from linearity is the CI threshold. Although a more robust and repeatable methodology would have been to analyze the derivative of the axial stress – lateral strain curve, this was not done here as the purpose of this paper is to compare the CVSR and ITLS approaches rather than to establish a new methodology for determination of CI.

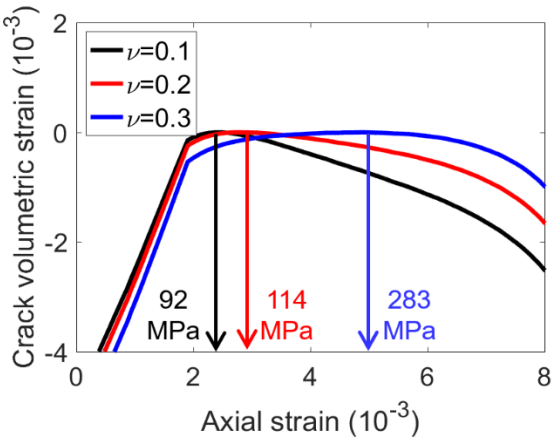

Fig. 2. Effect of ν on the point of CVSR.

3. CREIGHTON GRANITE

The granite selected for analysis is from Creighton mine located in Sudbury, Canada. Walton et al. (2016) previously characterized this rock on the basis of unconfined and confined compression test data. These tests were conducted on 120 mm x 55 mm circular specimens in a stiff loading system at CANMET laboratory in Canada. Creighton Granite has an average unconfined compressive strength (UCS) of 203 MPa and a tensile strength of 9 MPa. A Hoek-Brown fit (Hoek and Brown, 1980) to the compression and tensile strengths yielded m_i of 20.9 (Walton, 2014), which corresponds to high strain burst potential per Diederichs (2007). Sinha and Walton (2020) subsequently utilized the axial stress, axial strain and lateral strain data from unconfined and triaxial (σ_3=0-60 MPa) tests to determine the CI (ITLS approach) and CD thresholds and re-evaluate the Poisson's ratio. For the purposes of this study, CIs were determined using the CVSR approach and have been compared to those in Sinha and Walton (2020).

Figure 3 shows the ITLS-based and CVSR-based CIs. Note that the ITLS-based CIs have been translated to the right by 1 MPa for visualization purposes. A linear fit is employed in this case as well as in the subsequent sections because such a trend was previously observed from micro-seismic data in Lac du Bonnet granite (Martin, 1997). The ITLS and CVSR provide close estimates of CI at σ_3=0 MPa (although ITLS-based CI was found to be consistently higher than CVSR-based CI under unconfined conditions and was statistically different with a $p<0.0001$ for Student's t-test) but diverge for increasing confining stress. While this might seem counter-intuitive to the trend associated with the CD threshold, i.e. volumetric strain reversal occurs at a greater stress level than the point of non-linearity in axial stress – axial strain curve in confined tests (Diederichs, 2003), it must be recalled that there is no inelastic axial deformation in the specimen at this point. The divergence is likely related to the low estimation of Poisson's ratio, which in this case was based on the initial linear section of the axial stress – lateral strain curve. When Poisson's ratio is estimated from the initial portion of the axial stress – lateral strain curve and that curve is non-linear right from the start of the test, inelastic volume change in the specimen (or CI) must correspond to a relatively low stress level.

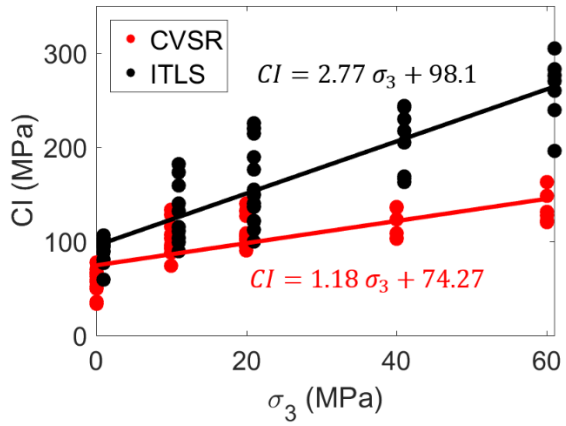

Fig. 3. CI thresholds of Creighton Granite determined using the CVSR and ITLS approaches.

When no linear region could be identified in the axial stress - lateral strain curve, especially in the high confinement tests, the region immediately ensuing the hydrostatic loading phase was selected for computing the Poisson's ratio. This is illustrated in Figure 4 a and b, in context of σ_3=60 MPa triaxial stress-strain curves (this is the highest level of confinement at which the rocks were tested). The methods followed for selecting the CI using the ITLS and CVSR approaches for this test are also illustrated in Figure 4c and d. The ITLS is an inverse measure of the slope of the axial stress – lateral strain curve and a linear increase in ITLS therefore implies a decrease in slope. From Figure 4c, it can be seen that there is no constant ITLS section, meaning that the slope of the axial stress – lateral strain started to change as soon as the deviatoric stress was applied to the specimen. The lack of a linear region is the primary source of the difficulty in

estimating a Poisson's ratio in triaxial compression tests and the subjectivity involved in the CVSR approach.

The selection of CI in this case was based on the change in linearity of the ITLS values (Figure 4c), which is mathematically equivalent to a change in the curvature of the axial stress – lateral strain curve. A similar approach was followed by Ghazvinian (2010) for determining the CI for Stanstead Granite. The exact mechanism by which the slope of the axial stress – lateral strain curve can decrease continually without the occurrence of additional irreversible damage (extensile microcracking) is not well understood. It is possible that the vertical pre-existing cracks that close during the hydrostatic loading phase start to open as soon as the deviatoric stress is applied to the specimen, manifesting in a non-linear lateral response from the start of deviatoric loading. The fact that the CI determined from acoustic emissions corresponds well with that from the ITLS approach in Ghazvinian (2010) further supports this proposition.

The crack volumetric strain reversal approach predicts a CI of 120 MPa that is less than 50% of the ITLS-based CI value. As discussed above, this is caused by the low estimate of ν. One can expect the CI to increase with increase in ν (Ghazvinian, 2010); increase in ν reduces the elastic component of volumetric strain (refer equation 2) and raises the crack volumetric strain to the limit when crack volumetric strain becomes equal to volumetric strain at ν of 0.5.

4. UTAH COAL

In this section, we utilized the compression test data on Utah coal, analyzed and documented previously by Kim et al. (2018). Uniaxial and triaxial tests were conducted on 44 mm diameter specimens with different cleat orientations (with respect to the longitudinal axis of the specimen) but only the 0° cleat data were considered here. In addition to the 0° dataset in Kim et al. (2018), some

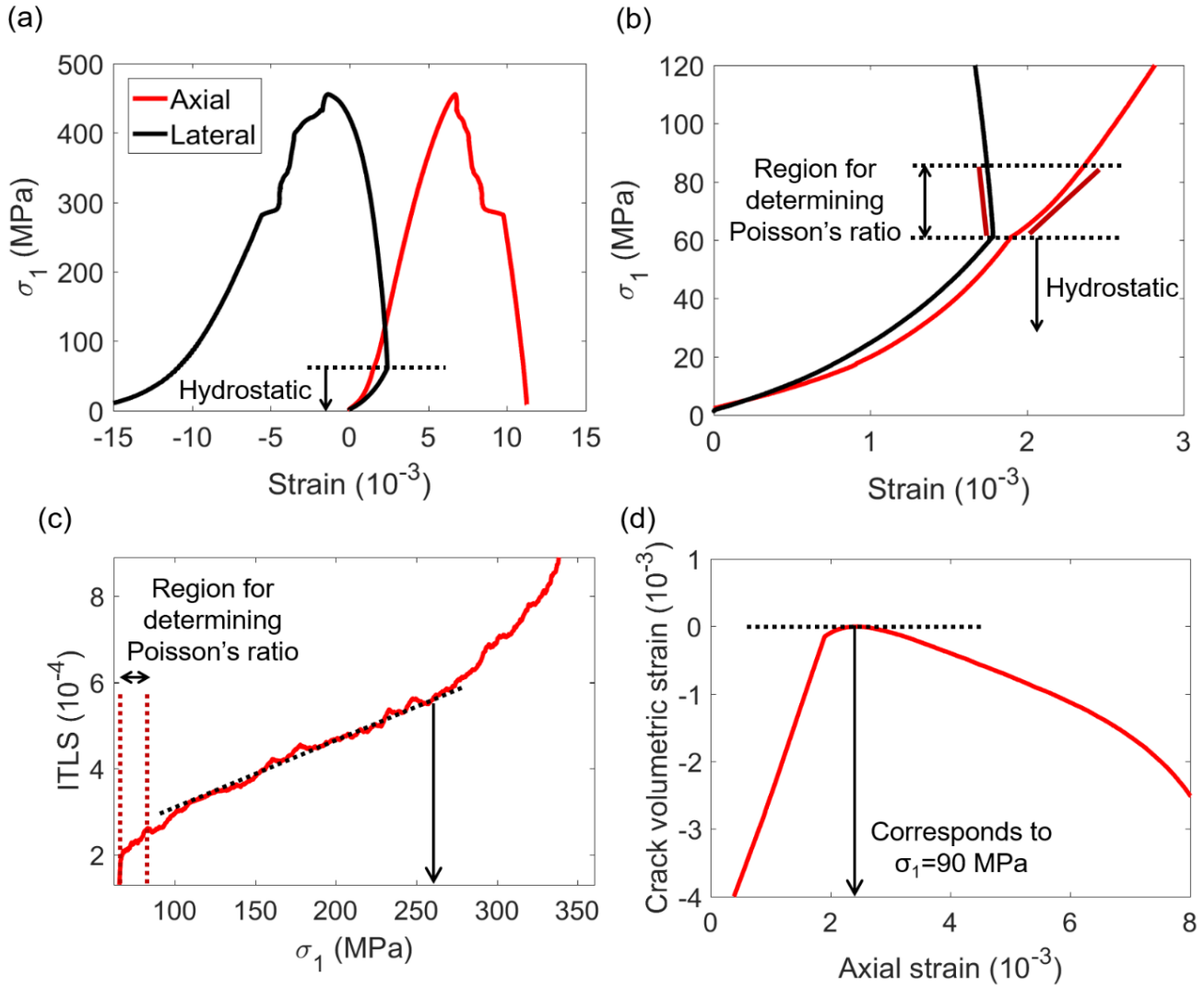

Fig. 4. (a) Stress-strain curve for a σ_3 = 60 MPa triaxial test, (b) Zoomed in-view of the stress-strain curve in (a) to show the region selected for determining Poisson's ratio in cases where the axial stress – lateral strain curve is non-linear from the start of the deviatoric loading phase. The regions are also highlighted by dotted maroon lines. (c) ITLS versus axial stress, and, (d) CVS versus axial strain.

high confinement data (σ_3 >12 MPa) were also included for broadening the scope of this study. The CI thresholds were determined using the CVSR and ITLS approaches and the results can be found in Figure 5. Similar to Figure 3, a divergent trend was noted, with the ITLS approach estimating a 55% higher CI than the CVSR approach at σ_3=110 MPa. Slight mismatch was observed in the CI values under unconfined conditions (statistically different means). The Poisson's ratio was again based on the initial linear section of the axial stress – lateral strain curve, where available; otherwise, it was based on the region immediately following the hydrostatic loading phase (as in Figure 4b).

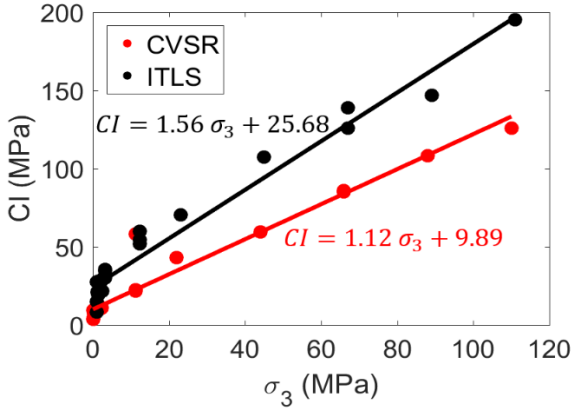

Fig. 5. CI thresholds of Utah coal determined using the CVSR and ITLS approaches. The ITLS datapoints have been translated to the right by 1 MPa for better visualization.

The ITLS versus axial stress and the CVS versus axial strain for a σ_3 = 11.2 MPa triaxial test are shown in Figure 6 to further emphasize the discrepancy. A continued increase in the ITLS value immediately past the hydrostatic loading phase can be noted. The point where the ITLS departed from linearity is the CI, which in this case is at σ_1=51.7 MPa. The CVSR, on the other hand, occurred at 22.8 MPa – a 56% drop with respect to the ITLS-based CI. With regards to Figure 6a, no identifiable change in the ITLS slope occurred at 22.8 MPa that can be related to systematic extensile cracking. A similar behavior was observed in all other confined tests.

The identical trends in the CI data for Creighton Granite and Utah coal might be related to their brittle character. A popular index for measuring material brittleness is the Hoek Brown curve fit parameter m_i (Diederichs et al., 2007; Kahraman et al., 2018) – a larger value implies more brittleness. For Creighton Granite, m_i is equal to 20.9 (Walton, 2014) while for Utah Coal, it ranges from 15 to 20 for cleat angles of 0° - 45° (Kim et al., 2016). Such high brittleness for both rock types imply that the brittle-to-ductile transition (Mogi, 1966) would occur at large confining stresses (Kim et al., 2019); consequently, fully ductile stress-strain behaviors were not observed in any of the aforementioned tests (even at σ_3=110 MPa in coal).

5. INDIANA LIMESTONE

Indiana Limestone is a Mississippian age carbonate rock, with a grain size of approximately 0.3-0.5 mm and a mean porosity of 14.8%. Walton et al. (2017) previously analyzed the stress-strain curves of Indiana limestone (σ_3=0-60 MPa) to understand how the post-yield strength and dilatancy evolves across the brittle-ductile transition. That study found σ_3=30 MPa, equivalent to σ_1/σ_3~5, to mark the transition between the brittle and ductile domain, and accordingly, ductile/strain-hardening responses were obtained in the σ_3>30 MPa tests. When deformations become increasingly ductile, pore collapse plays a more important role than microcracking, leading to an initial compactant stage in carbonate rock deformation (Wong and Baud, 2012). However, as the specimen is loaded continually, the behavior ultimately becomes more dilatant at large strains.

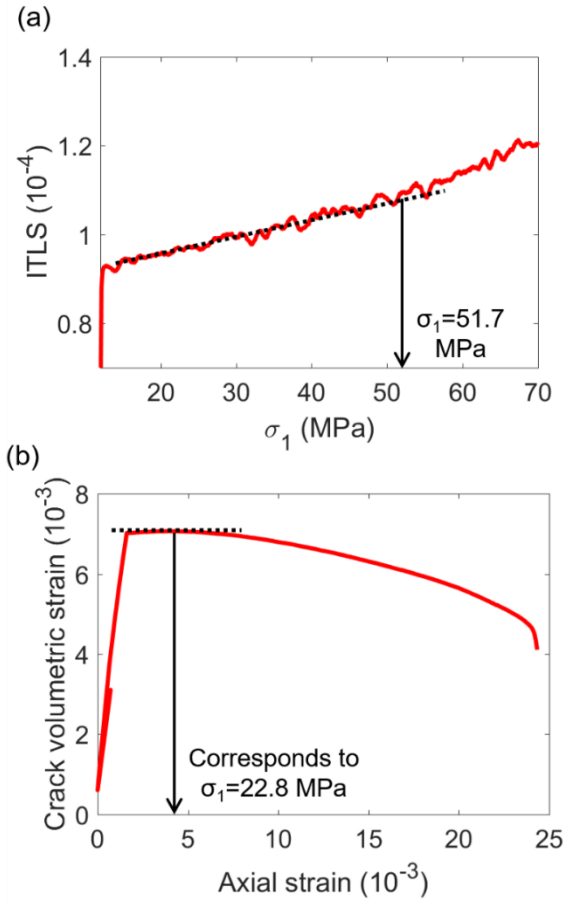

Fig. 6. (a) ITLS versus axial stress, (b) CVS versus axial strain for a σ_3 = 11.2 MPa triaxial test.

For the purposes of the current study, CI was re-evaluated from the Indiana Limestone stress-strain curves using the ITLS and CVSR approaches. Figure 7 graphically illustrates these two approaches in the context of a UCS test and two triaxial tests with the confining stresses at 20

MPa and 50 MPa. It follows from the previous discussion that the UCS and σ_3=20 MPa tests are in the brittle regime while the σ_3=50 MPa test is in the ductile regime. From the ITLS approach, two different CIs were determined (termed as 1 and 2) – one corresponds to the termination point of the plateau while the other corresponds to the point where the ITLS becomes non-linear. Recall that it is the second point (or 2) that was considered as CI in the two previous sections. In the CVSR approach, the CVS curves from the triaxial tests had to be translated in order to align the peak point with 0 crack volume strain (refer to Figure 7d, f).

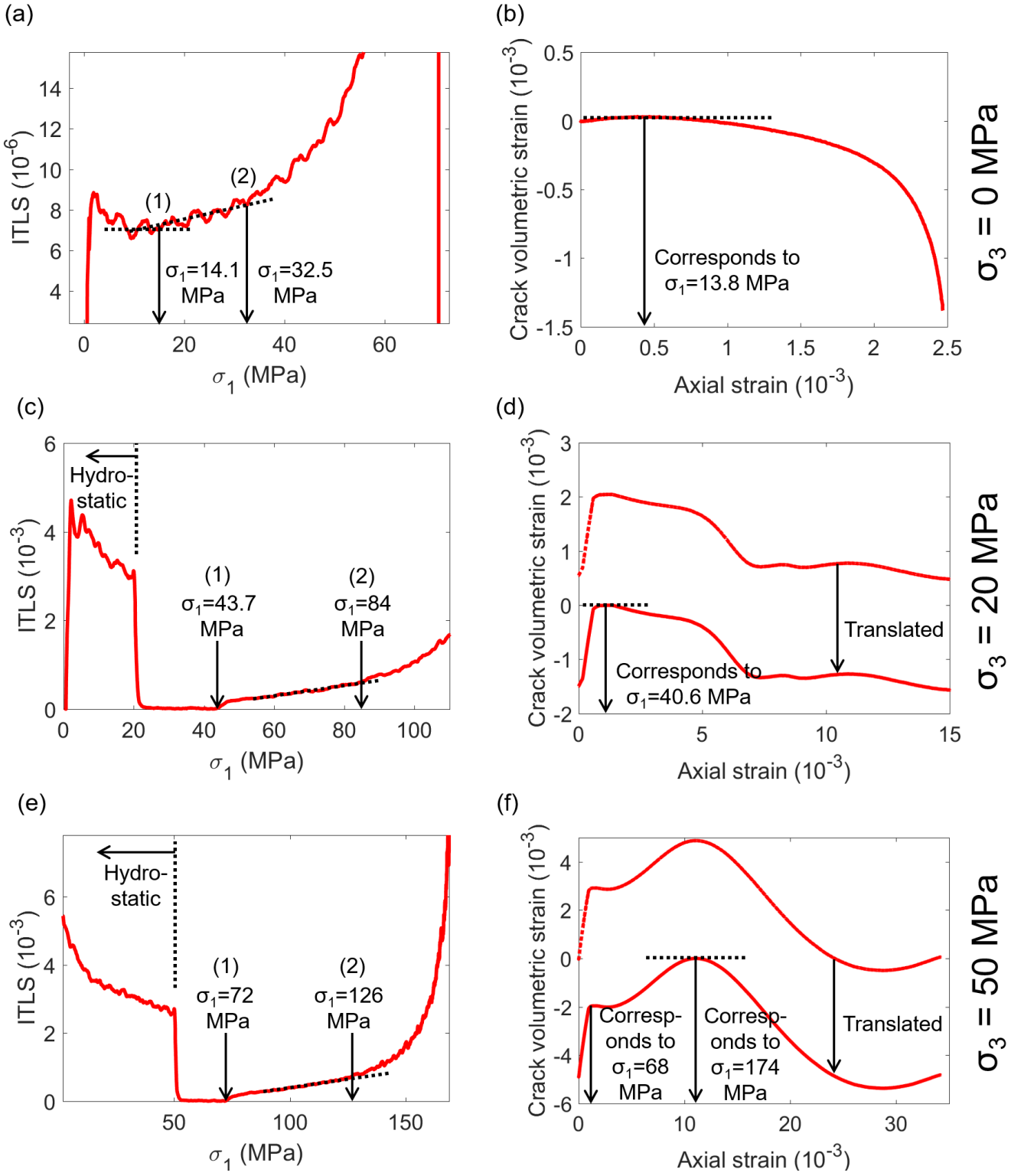

Fig. 7. ITLS versus axial stress for (a) σ_3 = 0 MPa, (c) σ_3 = 20 MPa, (e) σ_3 = 50 MPa triaxial tests, and, CVS versus axial strain for (b) σ_3 = 0 MPa, (d) σ_3 = 20 MPa, (f) σ_3 = 50 MPa triaxial tests.

The ITLS (1) point seemed to align with the CVSR point in the UCS and σ_3=20 MPa tests, but a mismatch was noted in the σ_3=50 MPa test. In particular, two peaks were observed in the σ_3=50 MPa test, with the first peak occurring at a stress level close to the ITLS (1) point. Double peaks were also noted in the σ_3=40 MPa and σ_3=60 MPa tests (Walton et al., 2017), and in such a scenario, the global maximum was chosen as the CI. The double peaks were not observed in the low confinement tests (see Figure 7b, d) implying that this is related to the ductile deformation processes.

Strangely enough, a near-perfect elastic change in the lateral strain occurred right after the hydrostatic loading phase ('plateau' before ITLS (2)). This 'plateau' was found in all the confined tests, even at σ_3=2 MPa. It was in this section that the Poisson's ratio was determined in Walton et al. (2017) and in this study. Since the 'plateau' region is preceded by compaction (closure of pre-existing cracks, pore collapse, etc.), it is possible there was a significant drop in porosity due to hydrostatic loading and subsequent application of deviatoric loading produced 'true' elastic response. With the discussions in previous sections in mind, the rise of ITLS at (1) and the continued linear response could be related to the re-opening of the pre-existing cracks. The fact that the slope of ITLS is steeper in the hydrostatic loading phase than in the linear region supports this notion – the closed pores cannot re-open with as much ease as can the pre-existing cracks.

The predominance of pore closure in the ductile regime can be readily observed from the σ_3 = 50 MPa test result (Figure 7e, f). Once the ITLS (1) stress level was attained in this test, there was a slight drop in the CVS value (dilation) triggered by an increase in lateral strain. Following that, the ITLS increased (lateral dilation) in a linear fashion but the crack volume continued to decrease (CVS increased). This is counterintuitive but can be explained by the greater contribution of pore collapse towards the crack volume strain than the opening of pre-existing cracks (Wong and Baud, 2012). It is only when the ITLS has started to increase in a non-linear fashion, i.e. formation and dilation of new extensile cracks, that the crack volume strain exhibits dilatancy. Clearly, the mechanisms involved in the deformation of a porous, less brittle (m_i=7.1; Walton et al., 2015) carbonate rock in the ductile regime is different than those in the brittle granite and coal.

The CIs determined from the two approaches are summarized in Figure 8 (a modified Boltzmann sigmoid curve was fitted to CVSR, as in Walton et al., 2017). The following observations can be made: (a) ITLS (1) occurred at a lower stress level than ITLS (2) and CVSR; (b) Even at σ_3=0, ITLS (2) consistently occurred at a higher stress level in comparison to CVSR; (c) Prior to 30 MPa confining stress, ITLS (2) estimated greater CIs than CVSR but the trend reversed as soon as the specimens were loaded past the brittle-ductile transition. This is likely attributed to a change in deformation mechanisms as discussed above. Based on these results, it seems that ITLS might be a better approach for determining CI under high confinements, especially because it considers the lateral response of the specimen only. At CI, cracking occurs mainly along the major principal stress direction (Diederichs, 2007) and any lateral strain-based approach should therefore yield accurate CI estimates. On the contrary, CVSR involves the entire volume of the specimen and therefore has the potential to erroneously estimate CI if the volume is influenced by inelastic deformation mechanisms occurring along the longitudinal axis of the specimen.

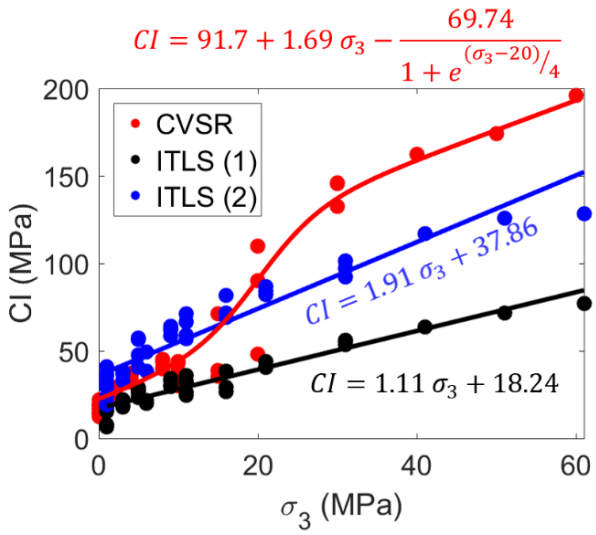

Fig. 8. CI thresholds of Indiana Limestone determined using the CVSR and ITLS approaches. The ITLS datapoints have been translated to the right by 1 MPa for better visualization.

6. CONCLUSIONS

This study has compared the CI thresholds determined using the crack volumetric strain reversal (CVSR) approach and the inverse lateral tangent stiffness (ITLS) approach for a granite, a coal and a limestone. A summary

Table 1. CIs determined using the two approaches for the three rock types.

Methodology	Creighton Granite	Utah Coal	Indiana Limestone
CVSR	1.18 σ_3 + 74.2	1.12 σ_3 + 9.9	91.7 + 1.69 σ_3 – 69.7 / (1 + e $^{(\sigma 3\text{-}20)/4}$)
ITLS (1)	2.77 σ_3 + 98.1	1.56 σ_3 + 25.7	1.11 σ_3 + 18.2
ITLS (2)			1.91 σ_3 + 37.9

of the CIs determined using the two approaches is provided in Table 1.

The following conclusions were drawn:

1. For the coal and the granite, the ITLS approach yielded higher CI thresholds in comparison to the CVSR approach, and the discrepancy increased with increase in confinement.

2. In cases where the axial stress – lateral strain curve was non-linear right from the start of the test (mostly in triaxial tests), the ITLS (mathematically equivalent to the inverse of stiffness) was initially linear with a positive slope. The point where the ITLS departed from linearity was chosen as CI. The initial linear increase in ITLS, indicating an expansion of the specimen diameter, was thought to be caused by reopening of the pre-existing cracks under deviatoric loading.

3. For the confined Indiana limestone tests, a constant ITLS section was observed after the hydrostatic loading phase. This was followed by an upward linear section, ultimately becoming non-linear at higher stresses. Although the end of the constant section (start of inelastic lateral strain) should ideally be the CI threshold, we considered both this point as well as the start of non-linearity to be possible CIs.

4. When the Indiana Limestone specimens were loaded in the ductile regime, two peaks were observed in the crack volume strain values; accordingly, the global maximum was chosen as CI. The CVSR-based CI was much higher than the two potential CIs obtained using the ITLS approach. In the brittle regime, however, the ITLS approach (the point of non-linearity) predicted higher CIs than the CVSR approach in Indiana Limestone, similar to the trend observed in the coal and the granite. The reversal in trend across the brittle-ductile transition likely occurred due to a change in deformation mechanisms.

5. From Table 1, it can be seen that there is a significant discrepancy in the CIs determined using the two approaches. If acoustic emission or ultrasonic techniques are unavailable, the authors recommend using the ITLS approach, as it is more direct methodology for CI determination. The ability of the ITLS approach to estimate CIs similar to those from acoustic emission was previously demonstrated by Ghazvinian (2010).

ACKNOWLEDGEMENT

The research conducted for this study was funded by the National Institute for Occupational Safety and Health (NIOSH) under Grant Number 200-2016-90154. The authors would like to extend their gratitude for the financial support. Special thanks to Dr. Mark K. Larson for reviewing this manuscript prior to submission and providing valuable suggestions.

DISCLAIMER

The findings and conclusions in this report are those of the authors and do not necessarily represent the views of the National Institute for Occupational Safety and Health. Mention of any company or product does not constitute endorsement by NIOSH.

REFERENCES

1. Andersson J.C. and C.D. Martin. 2009. The Äspö pillar stability experiment: Part I—Experiment design. *International Journal of Rock Mechanics and Mining Sciences*, 46(5), 865-78.
2. Andersson J.C. and C.D. Martin, H. Stille. 2009. The Äspö pillar stability experiment: part II—rock mass response to coupled excavation-induced and thermal-induced stresses. *International Journal of Rock Mechanics and Mining Sciences*, 46(5), 879-95.
3. Bieniawski Z.T. and M.J. Bernede. 1979. Suggested methods for determining the uniaxial compressive strength and deformability of rock materials: Part 1. Suggested method for determining deformability of rock materials in uniaxial compression. *International Journal of Rock Mechanics and Mining Sciences & Geomechanics Abstracts*, 16(2), 137-138.
4. Diederichs M.S. and C.D. Martin. 2010. Measurement of spalling parameters from laboratory testing. In: Zhao Labiouse, Dudt, Mathier eds. *Rock Mechanics in Civil and Environmental Engineering*. London: Taylor & Francis, 323-326.
5. Diederichs M.S. 2006. Rock fracture and collapse under low confinement conditions. *Rock Mechanics and Rock Engineering*, 36(5), 339-81.
6. Diederichs M.S. 2007. The 2003 Canadian Geotechnical Colloquium: Mechanistic interpretation and practical application of damage and spalling prediction criteria for deep tunnelling. *Canadian Geotechnical Journal*, 44(9), 1082-116.
7. Diederichs M.S., J.L. Carvalho and T.G. Carter. 2007. A modified approach for prediction of strength and post yield behaviour for high GSI rockmasses in strong, brittle ground. In *Proceedings of the 1st Canada-US Rock Mechanics Symposium*, 249–57.
8. Eberhardt E., D. Stead, B. Stimpson and R.S. Read. 1998. Identifying crack initiation and propagation thresholds in brittle rock. *Canadian Geotechnical Journal*, 35(2), 222-33.
9. Fairhurst C.E. and J.A. Hudson. 1999. Draft ISRM suggested method for the complete stress-strain curve for intact rock in uniaxial compression. *International Journal of Rock Mechanics and Mining Science*, 36(3), 279-89.
10. Ghazvinian E. 2010. *Modeling and testing strategies for brittle fracture simulation in crystalline rock samples*. M.A.Sc Thesis, Queen's University, Ontario, Canada.
11. Ghazvinian E. 2015. *Fracture initiation and propagation in low porosity crystalline rocks:*

implications for excavation damage zone (EDZ) mechanics. Doctoral dissertation, Queen's University, Kingston, Canada.

12. Hoek E. and E.T. Brown. 1980. Empirical strength criterion for rock masses. *Journal of Geotechnical and Geoenvironmental Engineering*, 106.
13. Hudson J.A., S.L. Crouch and C. Fairhurst. 1972. Soft, stiff and servo-controlled testing machines: A review with reference to rock failure. *Engineering Geology*, 6(6), 155–189.
14. Kahraman S., O.Y. Toraman and S. Cayirli. 2018. Predicting the strength and brittleness of rocks from a crushability index. *Bull Eng Geol Env*, 77, 1639–45.
15. Kim B.H., G. Walton, M.K. Larson and S. Berry. 2018. Experimental study on the confinement-dependent characteristics of a Utah coal considering the anisotropy by cleats. *International Journal of Rock Mechanics and Mining Sciences*, 105, 182-91.
16. Kim B.H., G. Walton, M.K. Larson and S. Berry. 2019. Investigation of the anisotropic confinement-dependent brittleness of a Utah Coal. *International Journal of Rock Mechanics and Mining Sciences*. (Under review).
17. Martin C.D. and N.A. Chandler. 1994. The progressive fracture of Lac du Bonnet granite. *International Journal of Rock Mechanics and Mining Sciences & Geomechanics Abstracts*, 31(6), 643-659.
18. Martin C.D. 1997. Seventeenth Canadian geotechnical colloquium: the effect of cohesion loss and stress path on brittle rock strength. *Canadian Geotechnical Journal*, 34(5), 698-725.
19. Martin C.D. and R.S. Read. 1996. AECL's Mine-by Experiment: A test tunnel in brittle rock. In *Proceedings of the 2nd North American Rock Mechanics Symposium*: NARMS'96, a Regional Conference of ISRM, Montréal, Québec, Canada, 1(13).
20. Mogi K. 1966. Pressure dependence of rock strength and transition from brittle fracture to ductile flow. *Bulletin Earthquake Research Institute*, 44, 215-32.
21. Peng J., G. Rong and M. Jiang. 2018. Variability of crack initiation and crack damage for various rock types. *Arabian Journal of Geosciences*, 11(11), 265.
22. Perras M.A. and M.S. Diederichs. 2016. Predicting excavation damage zone depths in brittle rocks. *Journal of Rock Mechanics and Geotechnical Engineering*., 8(1), 60-74.
23. Reed R.S. 2004. 20 years of excavation response studies at AECL's Underground Research Laboratory. *International Journal of Rock Mechanics and Mining Sciences*, 41, 1251-1275.
24. Sinha S. and G. Walton. 2020. A study of Bonded Block Model (BBM) complexity for simulation of laboratory-scale stress-strain behavior of granitic rocks. *Computers and Geotechnics*, 118, 103363.
25. Walton G. 2014. *Improving continuum models for excavations in rock masses under high stress through an enhanced understanding of post-yield dilatancy.* Doctoral dissertation, Queen's University, Kingston, Canada.
26. Walton G., J. Arzua, L.R. Alejano, M.S. Diederichs. 2015. A laboratory-testing-based study on the strength, deformability, and dilatancy of carbonate rocks at low confinement. *Rock Mechanics and Rock Engineering*, 48(3), 941-58.
27. Walton G., M.S. Diederichs, A. Punkkinen and J. Whitmore. 2016. Back analysis of a pillar monitoring experiment at 2.4 km depth in the Sudbury Basin, Canada. *International Journal of Rock Mechanics and Mining Sciences*, 85, 33-51.
28. Walton G., A. Hedayat, E. Kim and D. Labrie. 2017. Post-yield strength and dilatancy evolution across the brittle–ductile transition in Indiana limestone. *Rock Mechanics and Rock Engineering*, 50(7), 1691-710.
29. Wong T.F. and P. Baud. 2012. The brittle–ductile transition in porous rock: a review. *Journal of Structural Geology*, 44, 25–53.
30. Zhao X.G., M. Cai, J. Wang and L.K. Ma. 2013. Damage stress and acoustic emission characteristics of the Beishan granite. *International Journal of Rock Mechanics and Mining Sciences*, (64), 258-69.